American Journal of Nanosciences
2016; 2(1): 1-7
http://www.sciencepublishinggroup.com/j/ajn
doi: 10.11648/j.ajn.20160201.11

Hydrothermal Synthesis, Physico-Chemical Characterization and Electrochemical Behavior of β-MnO_2 Nanorods

Afef Bayoudh[1], Noureddine Etteyeb[1], Faouzi Sediri[1, 2, *]

[1]Unité de recherche de Nanomatériaux et Environnement (UR15ES01), IPEIT, Université de Tunis, Tunisie, Tunisia

[2]Département de Chimie, Faculté des Sciences de Tunis, Université Tunis El Manar, Tunisie, Tunisia

Email address:

faouzi.sediri@fst.utm.tn (F. Sediri)

[*]Corresponding author

To cite this article:

Afef Bayoudh, Noureddine Etteyeb, Faouzi Sediri. Hydrothermal Synthesis, Physico-Chemical Characterization and Electrochemical Behavior of β-MnO_2 Nanorods. *American Journal of Nanosciences*. Vol. 2, No. 1, 2016, pp. 1-7. doi: 10.11648/j.ajn.20160201.11

Received: August 30, 2016; **Accepted**: October 7, 2016; **Published**: October 17, 2016

Abstract: A simple hydrothermal method was developed for the synthesis ofpyrolosite β-MnO_2 nanorods, using potassium permanganate ($KMnO_4$), manganese sulfate ($MnSO_4.H_2O$) and oxalic acid ($H_2C_2O_4$). The effects of the reaction time, the hydrothermal temperature and the amount of $H_2C_2O_4$ on the structure and the morphology of the final products were studied. The β-MnO_2 nanorods are up to several micrometers in length and about 37 nm in average diameter. The samples were analyzed through X-ray diffraction (DRX), scanning electron microscopy (SEM), Fourier-transform infrared spectroscopy (FTIR) and Raman spectroscopy. Electrochemical measurements of thin film of β-MnO_2 nanorods have revealed reversible redox behavior with charge-discharge cycling processes corresponding to reversible cations intercalation/deintercalation into the crystal lattice. This process is easier for the small Li^+ to the larger Na^+ one and to the largest K^+ cation.

Keywords: Nanostructures, Hydrothermal Synthesis, X-ray Diffraction, Electrochemical Properties

1. Introduction

In recent years, construction of nano-sized transition metals oxides (ZnO, VO_2, MoO_2,WO_3, MnO_2, …) with different shapes including needles, rods, wires, spindles, tubes,… have attracted much attention [1-5].These materials were widely applied in the fields of catalysis [6], supercapacitors [7], lithium ion-batteries [8] and magnetic materials [9]. Among these materials, the manganese oxide MnO_2, as one of the most important transition metals oxides, has drawn particular attention owing to its high activity, low cost and nontoxicity [10-16]. It has various polymorphic structures, such as α-, β-, γ- and δ- types [17-20], which are made of the basic unit [MnO_6] octahedral with different connectivity.β-MnO_2 (pyrolosite) has a rutile type-tetragonal symmetry ($P4_2/mnm$) with (1 × 1) tunnel structure constructed of single type chain with edge-sharing [MnO_6] octahedral as illustrated in figure 1 [21]. Owing to its particular properties, β-MnO_2 is a traditionally attractive material for various industrial applications. It is an important battery cathode material used for lithium ion- batteries [22], sodium ion- batteries [23] and supercapacitors [24].

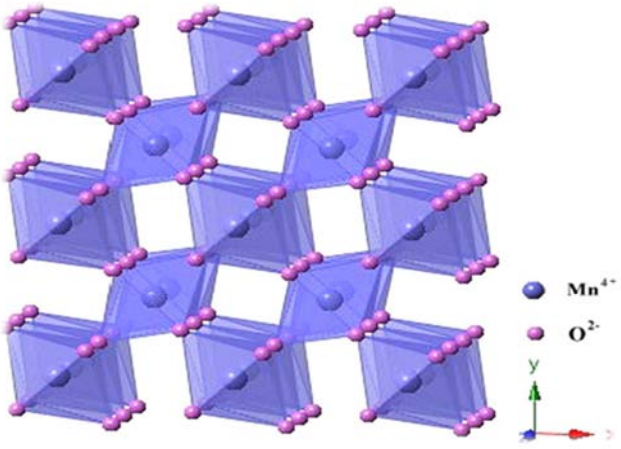

Figure 1. *Crystal structure of β-MnO_2.Mn is located in octahedral sites.*

There are many reports on the usage of β-MnO_2

nanostructures as catalyst. For example, it was found that β-MnO_2nanomaterials had catalytic performance on H_2O_2 decomposition [25-27] and on the degradation of organic polluants in waste water [28]. Recently, this variety of β-MnO_2 nanostructured, with different morphologies, such as nanowires [29], nanopincers like [21], nanowhiskers [30], nanotubes [31], nanorods [32] and hollow bipyramid [33] have been synthesized. A variety of strategies have been designed to prepared desirableβ-MnO_2 with different shapes. β-MnO_2 nanorods were successfully prepared by a refluxing route using manganese sulfate ($MnSO_4$, H_2O), sodium persulfate ($Na_2S_2O_8$) and sodium hydroxide (NaOH) as the raw materials [34]. A simple hydrothermal method was developed for the synthesis of uniform single-crystal β-MnO_2nanorods only using potassium permanganate and sodium nitrite in acidic solution [35]. G. Xi et al. have prepared β-MnO_2 structures through a two-step process including the hydrothermal synthesis of γ-MnOOH nanorods precursors followed by calcinations of the fabricated precursor [36]. Y. Wu et al. have synthesized β-MnO_2 nanowires using $KMnO_4$ and $H_2C_2O_4$ via aqueous and hydrothermal routes [37].

In this paper, we described a simple one-pot hydrothermal synthesis of β-MnO_2 nanorods. Compared to other soft chemical routes, this technique could precisely control the morphology of the product only by adjusting the experimental conditions (such as reaction temperature, reaction times and reactant concentration). As far as we know the synthesis of β-MnO_2 nanorods using $KMnO_4$, $MnSO_4$. H_2O and $H_2C_2O_4$ under hydrothermal conditions had not been reported. We have investigated the effects of the hydrothermal temperature, reaction time and the amount of $H_2C_2O_4$ on the crystallographic structure and morphology of products. The optimal conditions for the preparation of homogeneous and high crystallized β-MnO_2 nanorods were described. The electrochemical properties of the β-MnO_2 nanorodsfilms deposited on indium tin-oxide (ITO)-coated glass have been investigated using cyclic voltammetry in the presence of Li^+, Na^+, and K^+ in propylene carbonate as electrolytic solution.

2. Experimental Section

2.1. Preparation of β-MnO_2 Nanorods

β-MnO_2 nanorods were synthesized through a hydrothermal process. Potassium permanganate $KMnO_4$ (≥ 99 %), manganese sulfate (II) monohydrate $MnSO_4.H_2O$ (98 +%) and oxalic acid anhydrous $H_2C_2O_4$ (98%) were purchased from Across Organics and are used without further purification.

The detailed synthesizing process was as follows. In a typical synthesis, 79 mg of $KMnO_4$and 86 mg of $MnSO_4.H_2O$ were dissolved in 10 mL of distilled water, then 45 mg of $H_2C_2O_4$ was added into the above solution under continuous stirring. The resulting suspension was transferred into a Parr Teflon-lined digestion bomb with a capacity of 45 mL which was sealed and maintained in an electric oven at different temperatures and various reaction times. After the bomb cooled down to room temperature, a black precipitate was obtained. The resulting precipitate was filtered and washed with distilled water and ethanol for several times and then dried in an electric oven at 60°C. Comparative experiments were carried out to investigate the influence of reaction time and temperature on the structure and the crystallinity of the samples, for that many experiments were carried out at 180°C during different times (1 hour, 2 hours, 4 hours, 6 hours and 24 hours). The other experiments we performed took place under varied reaction temperature, 120°C and 220°C, with a 24 hour -reaction time.

2.2. Characterization Techniques

X-ray powder diffraction data (XRD) were obtained on a X'Pert Pro Panalytical diffractometer with CuK_α radiation (λ = 1.5418Å) and graphite monochromator. The XRD measurements were carried out by applying a step scanning method (2θ range from 3° to 70°), with a scanning rate of 0.017° s^{-1} and a step time of1s. Scanning electron microscopy (SEM) studies were recorded with a JEOL JSM-5400 mocroscope. Fourier-transform infrared spectroscopy (FTIR) was recorded from 4000 to 400 cm^{-1} on a Nicolet 380 spectrometer in pellets of samples dispersed in KBr. Raman spectroscopy was performed using a Jobin Yvon T 64000 spectrometer(blue laser excitation with 488 nm wavelength and <55 mW power at the sample). The electrochemical measurements were carried out using one compartment cell and a BioLogic SP150 potentiostat/galvanostat apparatus. Ag/AgCl electrode and a stainless grid were used as reference and counter-electrode electrode, respectively. The working electrode is a film of β-MnO_2 nanorods deposited on a plate of indium tin oxide (ITO). The electrode was prepared thus: an aqueous suspension of 3 mg/mL of β-MnO_2 nanorods was prepared then 100 µL of this suspension were dropped onto a 1 cm^2 surface ITO coated glass (plate of indium tin oxide).The surface modified ITO coated glass was then dried and covered with 10 µL of a Nafion solution (obtained by dissolving in ethanol a commercial Nafion solution 9/1 V/V) used as working electrode. Lithium perchlorate 1M ($LiClO_4$), sodium perchlorate 1M ($NaClO_4$) and potassium perchlorate 1M ($KClO_4$) dissolving in propylene carbonate (PC) were used as electrolyte solutions. The operating voltage was controlled between -1.0 V and 1.0 V. All measurements were performed at different scan rates at room temperature.

3. Results and Discussion

3.1. X-ray Diffraction

The figure 2 contains the X-ray diffractgrams of the as-synthesized samples atdifferent temperatures: 120°C (a), 180°C (b) and 220°C (c) after 24 hours of hydrothermal treatment. Indeed, the diffraction pattern shows the presence of amorphous material, when the synthesis was carried at

120°C (figure 2a). However, when the synthesis was carried out at 180°C, the XRD pattern shown in figure 2b indicates that the diffraction peaks are identical to those of the tetragonal crystalline phase β-MnO_2 ($P4_2/mnm$) with lattice constant a= b = 4.397 Å and c = 2.867Å, according to the literature values (JCPDS#24-0735).No peak of any other phase or impurity was detected from the XRD pattern. Increasing the temperature to 220°C (figure 2c), the diffraction pattern shows the presence of β-MnO_2 (JCPDS #24-0735) with the presence of peaks which are characteristic of α-MnO_2 (JCPDS # 44-0141). It could be concluded that β-MnO_2 with high purity can be obtained via the hydrothermal treatment at 180°C for 24 hours.

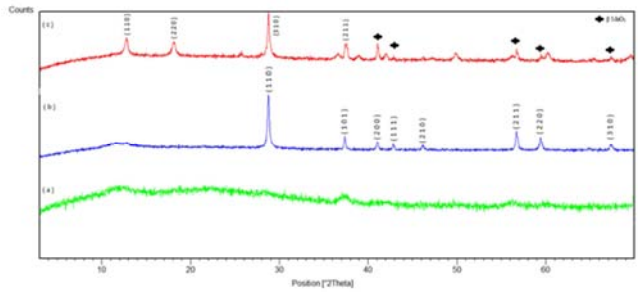

Figure 2. *XRD patterns of the samples synthesized for 24 hours at different reaction temperatures: 120°C (a), 180°C (b) and 220°C (c).*

The phase structure of the resulting samples prepared at 180°C for different reaction times: 1 hour (a), 2 hours (b), 4 hours(c), 6 hours (d) and 24 hours (e) were determined by X-ray powder diffraction (XRD), as shown in figure 3. Indeed, figure 3a shows the XRD pattern of the as-synthesized sample after 1 hour of hydrothermal treatment, it's an amorphous material. It was found that the crystallization starts after 2 hours (figure 2b) and improves when the reaction time increases, above 4, 6 and 24 hours at 180°C as shown in the figures 2c, 2d and 2e. In fact, strong and sharp diffraction peaks indicate good crystallinity of the hydrothermal product prepared after 24 hours at 180°C. The reaction temperature and time have a significant effect on the crystalline phase of tetragonal β-MnO_2.

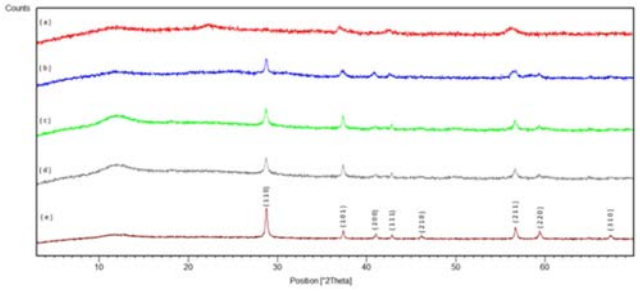

Figure 3. *XRD patterns of the samples synthesized at 180 °C for different reaction times: 1 hours (a), 2 hours (b), 4 hours (c), 6 hours (d) and 24 hours (e).*

To fully understand the effect of the introduction of $H_2C_2O_4$ on the crystallinity of β-MnO_2 nanostructures, we carried out an experiment of the hydrothermal process without oxalic acid ($H_2C_2O_4$), using only potassium permanganate ($KMnO_4$) and manganese sulfate ($MnSO_4.H_2O$) and the others experiments with the introduction of 45 mg and 150 mg of $H_2C_2O_4$. XRD patterns of the resulting samples synthesized without oxalic acid (figure 4b) and with 45 mg of oxalic acid (figure 4a), can be indexed as the tetragonal phase of β-MnO_2, while the sample prepared using 150 mg of $H_2C_2O_4$ (figure 5) can be identified to be a pure manganite γ-MnOOH phase with lattice parameters a= 5.300 Å, b=5.278 Å, c= 5.300 Å, α = γ = 90° and β = 114.36° according to JCPDS# 41-1379.

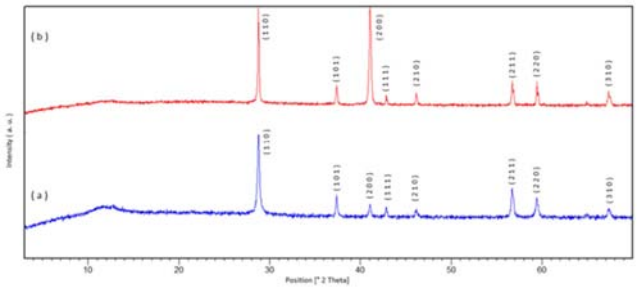

Figure 4. *XRD patterns of the samples synthesized with 45 mg of $H_2C_2O_4$ (a) and without $H_2C_2O_4$ (b).*

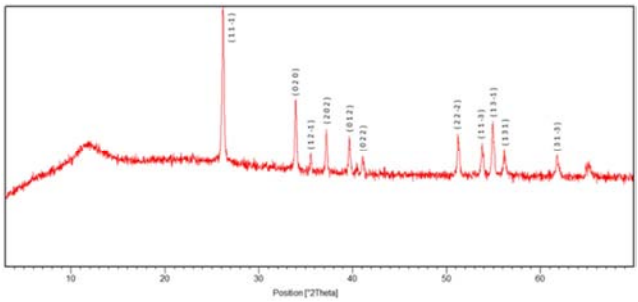

Figure 5. *XRD pattern of the sample synthesized with 150 mg of $H_2C_2O_4$.*

3.2. Scanning Electronic Microscopy

The morphology of the as-synthesized materials was investigated by using the scanning electron microscopy (SEM). Figure 6 shows SEM images of the β-MnO_2 synthesized at 180°C for 4 hours (a), 6 hours (b) and 24 hours (c). In fact, the reaction time plays an important role in controlling the morphologies of theMnO_2 nanostructures. When the hydrothermal reaction time is 4hours nanoparticules are obtained. The sample is homogenous and displays rod like morphology with a diameter of 88 nm and about 4 µm in length when it reaches 6 hours. Furthermore, with the increase of the reaction time to 24 hours, the product is mainly nanorods, but the nanorods became longer and thinner. They are 37 nm in diameter and about 6 µm in length.

To substantially study the influence of the amount of oxalic acid on the morphology of the samples prepared at 180°C for 24 hours, observations by scanning electron microscopy were performed. The observation by SEM of the as-synthesized sample without oxalic acid shows that the material is made of micro rods (figure 7a). Whereas, when

the synthesis was carried out with 150 mg of oxalic acid, figure 7b reveals that pure crystalline manganite γ-MnOOH was obtained in a large scale with a high uniformity, the as-prepared γ-MnOOH nanorods are up to 2 µm in length and about 30 nm in diameter.

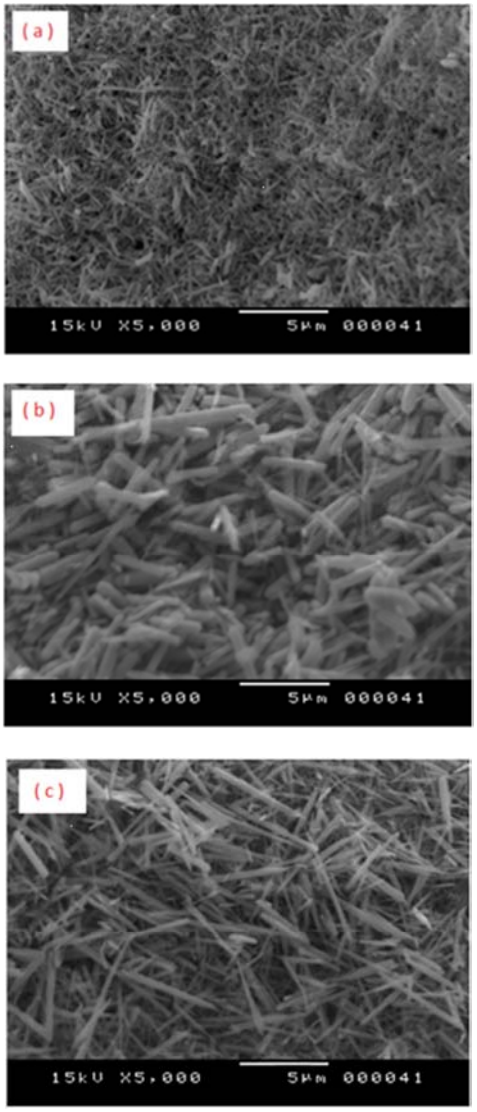

Figure 6. *SEM micrographs of the samples synthesized at 180°C for different reaction times: 4 hours (a), 6 hours (b) and 24 hours (c).*

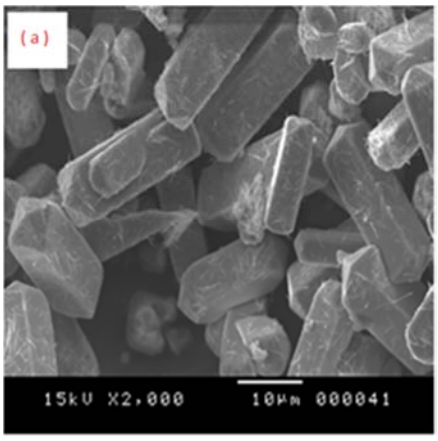

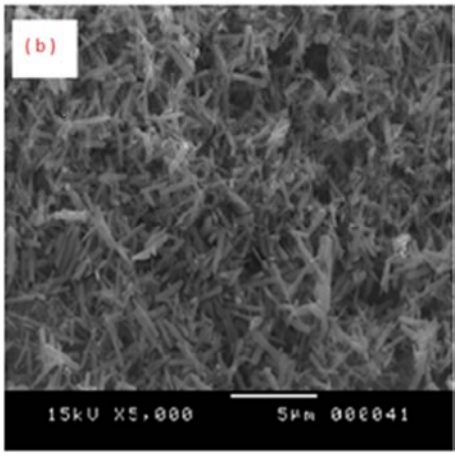

Figure 7. *SEM micrographs of the samples synthesized at 180°C for 24 hours: without $H_2C_2O_4$ (a) and with 150 mg of $H_2C_2O_4$ (b).*

3.3. Vibrational Spectroscopic Study

The vibrational spectroscopic methods, which include IR and Raman diffusion spectroscopy, afford useful alternatives and/or supplements to X-ray diffraction for structural characterizations of materials. Since they are sensitive to local structures of materials, IR and Raman diffusion spectroscopy can yield a more complete and reliable description of materials such as MnO_2-related compounds, where crystalline disorders as well as different local structural properties can be expected [38]. Thereby, figure 8 shows the FTIR spectrum of the β-MnO_2 nanorods prepared at 180°C for 24 hours recorded in the region 400-4000 cm^{-1}. All bands located at 417 cm^{-1}, 604 cm^{-1} and 720 cm^{-1}can be ascribed to the Mn-O vibrations of the rutile-type MnO_6 octahedral framework which confirms the formation of β-MnO_2 nanocrystals [39-41].

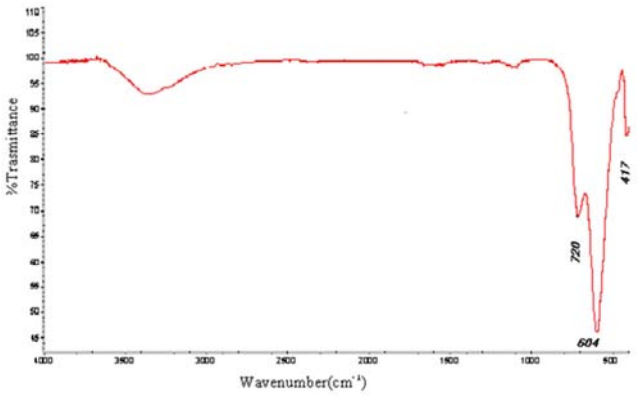

Figure 8. *FTIR spectrum of β-MnO_2 nanorods.*

Raman spectroscopy is known to be an appropriate technique for the investigation of the short-range order, phase structure. The Raman bands of MnO_2 are determined by the [MnO_6] octahedral environment; hence the use of Raman spectroscopy to identify the structure of the different crystalline phases. The Raman spectrum of β-MnO_2 nanorods (figure 9) displays 5 three sharp peaks at 538, 661 and 750 cm^{-1} assigned to the characteristic MnO_2 vibration modes.

Indeed, the peak observed at 661 cm^{-1} is assigned to the stretching mode Mn-O vibrations. Nevertheless, the two peaks located at 538 and 750 cm^{-1} can be assigned to the deformation modes of the metal-oxygen chain of Mn-O-Mn in the MnO_2 octahedral lattice [38, 42, 43].

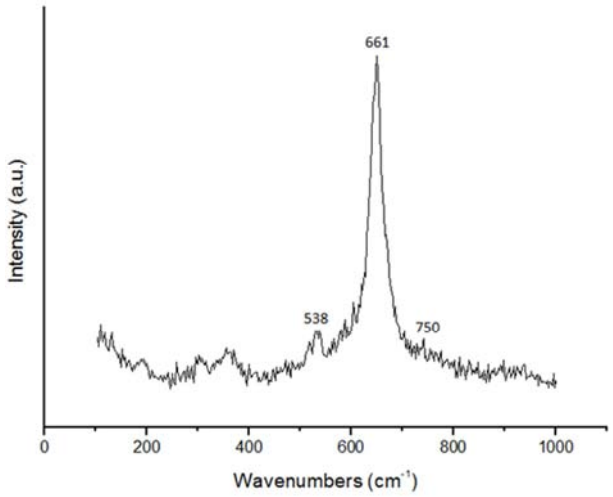

Figure 9. *Raman spectrum of β-MnO_2nanorods.*

3.4. Electrochemical Characterization

It was reported that the electrochemical properties of the electrode materials are influenced by many factors such as instinctive structure, morphology, and preparation processes [44]. Cyclic voltammetry curves shown in figure 10 were recorded from the 1st to the 50th cycles at room temperature with a scan rate of 50 mV/s in the range [-1.0 to 1.0 V] in 1 M$LiClO_4$ in propylene carbonate solution. The CV data are consistent with good stability of the as-prepared crystalline β-MnO_2nanorods coated film. The curves showed a single oxidation and reduction process. After several voltammetry cycles (50 cycles), the voltammetry responses remain unchanged (figure 10).The absence of even a minimal deviation from the anodic and cathodic peaks positions upon extending cycling confirms the absence of degradation problems which can affect the β-MnO_2 electrode. The voltammograms show the presence of a single redox process. The cathodic and anodic peaks at -0.70 V and 0.70 V can be attributed to intercalation/deintercalation process of Li^+ ions into the tunnel cavities of the sample, which mainly corresponds to the reduction of Mn^{4+} to Mn^{3+} and the oxidation of Mn^{3+} to Mn^{4+}, respectively. The cathodic and anodic peaks currents increased as the scan rate does (figure 11). This phenomenon indicates the dynamics of the lithium intercalation/deintercalation occurring in the material to provide electroneutrality. The electrochemical reaction can be written thus:

$$MnO_2 + xe^- + xLi^+ = Li_xMnO_2$$

The electron transfer during $Mn^{4+/}Mn^{3+}$ couple redox processes are accompanied by the insertion of Li^+ cation at reduction and by its release at oxidation of the material in order to equilibrate the charge.

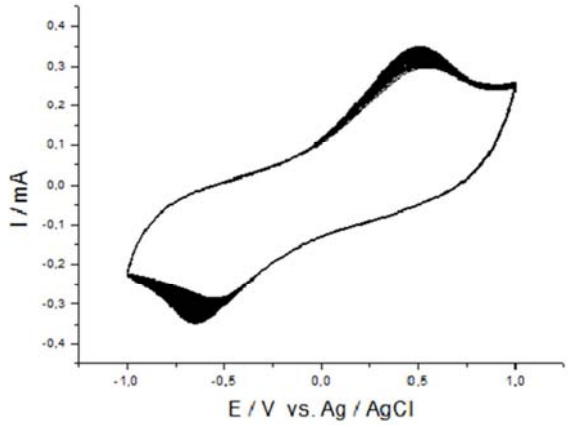

Figure 10. *Cyclic voltammetric curves of β-MnO_2 nanorods deposited on ITO-coated glass, recorded at 50 mV/s from 1 to 50th cycles in 1 M $LiClO_4$/PC.*

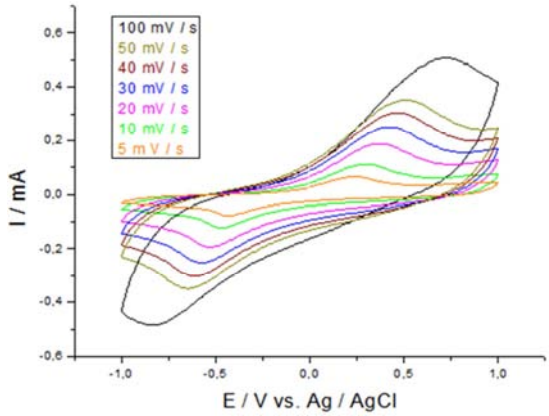

Figure 11. *Cyclic voltammetric curves of 1st cycle responses of β-MnO_2 nanorods deposited on ITO-coated glass, recorded at different scan rates (5, 10, 20, 30, 40, 50 and 100 mV/s) in 1 M $LiClO_4$/PC.*

The quantity of charges Q exchanged during the experiment can be deduced from the surface of cyclic voltammetry curves and the coulombic efficiency during the insertion/desinsertion release process can be expressed by the ratio Q_{red}/Q_{ox}. Figure 12shows that the value of the coulombic efficiency after several cycles is 87%. This indicates that the Li^+ intercalation-deintercalation is quasi-reversible at 50 mV/s scan rate. When the films of β-MnO_2 nanorods have been studied in propylene carbonate containing $NaClO_4$ or $KClO_4$ as electrolytes instead of $LiClO_4$ (figure 13), the reduction current peaks have increased upon medium transfer from K, Na^+ to Li^+ containing electrolyte. This observation indicates that intercalation/deintercalation processes involving K^+ and Na^+ are less effective and more difficult in comparison to those with Li^+ cations. It should be noted that the Vander Waals radius of K^+ and Na^+ are larger than that of Li^+ cation. In addition the diffusion process of cations is mainly controlled by the size of the tunnel. The tunnel size of β-MnO_2 (1.89 Å) is considerably larger than the radius of Li^+ (0.76 Å) and Na^+ (1.02 Å), but it is smaller than that of K^+ (1.33Å) [45]. The excellent stability of β-MnO_2 nanorods makes it an interesting possible future electrode for rechargeable lithium cell.

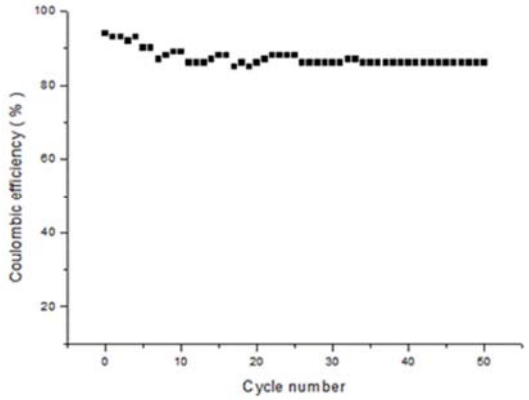

Figure 12. *Coulombic efficiency of β-MnO_2 nanorods recorded at 50 mV/s over 50 cycles.*

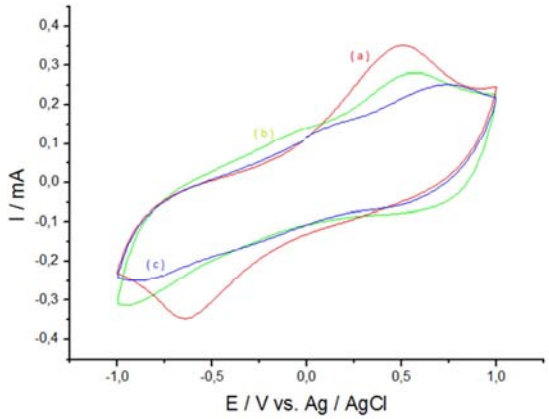

Figure 13. *Cyclic voltammetric curves of the 1st cycle responses of β-MnO_2 nanorods deposited on ITO-coated glass, recorded at 50 mV/s: in 1 M $LiClO_4$/PC (a), 1 M $NaClO_4$/PC (b) and in 1 M $KClO_4$/PC (c).*

4. Conclusion

β-MnO_2 nanorods were synthesized hydrothermally via a simple and elegant route from the mixture of $KMnO_4$, $MnSO_4.H_2O$ and $H_2C_2O_4$ under soft conditions. In fact the presence of $H_2C_2O_4$, the temperature and reaction times played an important role in the structure and the morphology of the final products. Electrochemical measurements carried out on thin film of β-MnO_2 nanorodsdeposited on ITO-modified glass electrodes have revealed quasi-reversible redox behaviors corresponding to partial reduction of manganese oxide, with charge-discharge cycling corresponding to the intercalation/deintercalation of Li^+ into the tunnel cavities of β-MnO_2 nanorods. The CV curves recorded in propylene carbonate medium ($LiClO_4$, $NaClO_4$ and $KClO_4$) show the presence of a single redox process. In fact, the CV curves indicate that the diffusion process involving Na^+ and K^+ is less effective and difficult. Thus, the redox process is more difficult for larger cations than for small ones. The presence of only one redox wave for each cation indicates that the dynamics of intercalation/deintercalation is the same and occurs mainly in the cavities. All these results indicate that the resulting β-MnO_2 nanorods are promising cathode materials in lithium-ion batteries.

References

[1] T. You, J. Yan, Z. Zhang, J. Li, J. Tian, J. Yun, W. Zhao, Fabrication and optical properties of needle-like ZnO array by a simple hydrothermal process, Mater. Lett. 66 (2012) 246-249.

[2] H. F. Xu, Y. Liu, N. Wei, S. W. Jin, From VO_2(B) toVO_2(A) nanorods Hydrothermal synthesis, evolution and optical properties in V_2O_5-$H_2C_2O_4$-H_2O system, Optik 125 (2014) 6078-6081.

[3] J. Zhou, N. S. Xu, S. Z. Deng, J. Chen, J. C. She, Synthesis of large-scaled MoO_2 nanowire arrays, Chem. Phys. Lett. 382 (2003) 443-446.

[4] D. J. Ham, A. Phuruangrat, S. Thongtem, J. S. Lee, Hydrothermal synthesis of monoclinic WO3 nanoplates and nanorods used as an electrocatalyst for hydrogen evolution reactions from water, Chem. Eng. J. 165 (2010) 365-369.

[5] H. Li, W.-L. Wang, F. Pan, X. Xin, Q. Chang, X. Liu, Synthesis of single-crystalline α-MnO_2 nanotubes and structural characterization by HRTEM. Mat. Sci. Eng. B–Solid 176 (2011) 1054-1057.

[6] Y. Zhu, M. Shen, Y. Xia, M. Lu, Au/MnO_2 nanostructured catalysts and their catalytic performance for the oxidation of 5-(hydroxymethyl)furfural, Catal. Commun. 64 (2015) 37-43.

[7] T. D. Dongale, P. R. Jadhav, G. J. Navathe, J. H. Kim, M. M. Karanjkar, P. S. Patil, Development of nano fiber MnO_2 thin film electrode and cyclic voltammetry behavior modeling using artificial neural network for supercapacitor application, Mat. Sci. Semicon. Proc. 36 (2015) 43-48.

[8] N. Li, W. Huang, Q. Shi, Y. Zhang, L. Song, A CTAB-assisted hydrothermal synthesis of VO_2(B) nanostructures for lithium-ion battery application, Ceram. Int. 39 (2013) 6199-6206.

[9] L. Li, J. Liang, H. Kang, J. Fang, M. Luo, X. Jin, TEA-assisted synthesis of single-crystalline Mn_3O_4 octahedrons and their magnetic properties, Appl. Surf. Sci. 261 (2012) 717-721.

[10] F. H. B. Lima, M. L. Calegaro, E. A. Ticianelli, Electrocatalytic activity of manganese oxides prepared by thermal decomposition for oxygen reduction, Electrochim. Acta 52 (2007) 3732-3738.

[11] Z. Liu, Y. Xing, C.-H. Chen, L. Zhao, and S. L. Suib, Framework Doping of Indium in Manganese Oxide Materials: Synthesis, Characterization, and Electrocatalytic Reduction of Oxygen, Chem. Mater. 20 (2008) 2069-2071.

[12] S. Shanmugam and A. Gedanken, MnO Octahedral Nanocrystals and MnO@C Core-Shell Composites: Synthesis, Characterization, and ectrocatalytic Properties, J. Phys. Chem. B 110 (2006) 24486-24491.

[13] V. M. B. Crisostomo, J. K. Ngala, S. Alia, A. Dobley, C. Morein, C.-H. Chen, X. Shen, and S. L. Suib, New Synthetic Route, Characterization, and Electrocatalytic Activity of Nanosized Manganite, Chem. Mater. 19 (2007) 1832-1839.

[14] K. Gong, P. Yu, L. Su, S. Xiong, and L. Mao, Polymer-Assisted Synthesis of Manganese Dioxide/Carbon Nanotube Nanocomposite with Excellent Electrocatalytic Activity toward Reduction of Oxygen, J. Phys. Chem. C111 (2007)1882-1887.

[15] S. F. Chin, S. C. Pang, M. A. Anderson, Self-assembled manganese dioxide nanowires as electrode materials for electrochemical capacitors, Mater. Lett. s 64 (2010) 2670-2672.

[16] M. R. Mahmoudiana, Y. Alias, W. J. Basirun, P. M. Woi, M. Sookhakian, Facile preparation of MnO_2 nanotubes/reduced graphene oxide nanocomposite for electrochemical sensing of hydrogen peroxide, Sensor. Actuat. B-Chem. 201 (2014) 526-534.

[17] M. M. Thackeray, Manganese oxides for lithium batteries, Progr. Solid. State Ch. 25 (1997) 1-71.

[18] J. Zhou, L. Yu, M. Sun, B. Lan, F. Ye, J. He, Q. Yu, MnO_2 Nanosheet-Assisted Hydrothermal Synthesis of β-MnO_2 Branchy Structures, Mater. Lett. 79 (2012) 288-291.

[19] M. Zhou, X. Zhang, L. Wang, J. Wei, L. Wang, K. Zhu, B. Feng, Growth Process and microwave absorption properties of nanostructured γ-MnO_2 urchins, Mater. Chem. Phys. 130 (2011) 1191-1194.

[20] X. Zhang, P. Yu, H. Zhang, D. Zhang, X. Sun, Y. Ma, Rapid hydrothermal synthesis of hierarchical nanostructures assembled from ultrathinbirnessite-type MnO_2nanosheets for supercapacitor applications, Electrochim. Acta 89 (2013) 523-529.

[21] G. Cheng, L. Yu, T. Lin, R. Yang, M. Sun, B. Lan, L. Yang, F. Deng, A facile one -pot hydrothermal synthesis of β-MnO_2 nanopincers and their catalytic degradation of methylene blue, J. Solid State Chem. 217 (2014) 57-63.

[22] X. Huang, D. Lv, Q. Zhang, H. Chang, J. Gan, Y. Yang, Highly crystalline macroporous β-MnO_2: Hydrothermal synthesis and application in lithium battery, Electrochim. Acta 55 (2010) 4915-4920.

[23] D. Su, H.-J. Ahn, and G. Wang, β-MnO_2 nanorods with exposed tunnel structures as high-performance cathode materials for sodium-ion batteries, NPG Asia Mater., 5 (2013) 70-77.

[24] J.-J. Zhu, L.-L. Yu, J.-T. Zhao, 3D network mesoporous Beta - manganese dioxide: Template-free synthesis and supercapacitive performance, J. Power Sources 270 (2014) 411-417.

[25] W. Zhang, Z. Yang, X. Wang, Y. Zhang, X. Wen, S. Yang, Large-scale synthesis of β-MnO_2 nanorods and their rapid and efficient catalytic oxidation of methylene blue dye, Catal. Commun. 7 (2006) 408-412.

[26] W. Zhang, H. Wang, Z. Yang, F. Wang, Promotion of H_2O_2 decomposition activity over β–MnO_2 nanorods catalysts, Colloid. Surface. A 304 (2007) 60-66.

[27] Z. Yang, Y. Zhang, W. Zhang, X. Wang, Y. Qian, X. Wen, S. Yang, Nanorods of manganese oxides: Synthesis, characterization and catalytic application, J Solid State Chem. 179 (2006) 679-684.

[28] Y. Dong, H. Yang, K. He, S. Song, A. Zhang, β-MnO_2 nanowires: A novel ozonation catalyst for water treatment, Appl. Catal. B: Environ. 85 (2009) 155-161.

[29] T. Zhang, X. Zhang, X. Yan, J. Ng, Y. Wang, D. D. Sun, Removal Of bisphenol A via a hybrid process combining oxidation on β-MnO_2 nanowires With microfiltration, Colloid. Surface. A 392 (2011) 198-204.

[30] X. Sun, C. Ma, Y. Wang, H. Li, Preparation and characterization of MnOOH and β-MnO_2 whiskers, Inorg. Chem. Commun. 5 (2002) 747-750.

[31] D. Zheng, S. Sun, W. Fan, H. Yu, C. Fan, G. Cao, Z. Yin and Xi. Song, One-Step Preparation of Single-Crystallineβ-MnO_2 Nanotubes, J. Phys. Chem. B 109 (2005) 16439-16443.

[32] G. Xi, Y. Peng, Y. Zhu, L. Xu, W. Zhang, W. Yu, Y. Qian, Preparation of β-MnO_2 nanorods through a γ-MnOOH precursor route, Mater. Res. Bull. 39 (2004) 1641-1648.

[33] X. Zheng, T. Lin, G. Cheng, B. Lan, M. Sun, L. Yu, Hollow bipyramid β-MnO_2: Pore size controllable synthesis and degradation activities, Adv. Powder Technol. 26 (2015) 622-625.

[34] X.-M. Liu, S.-Y. Fu, C.-J. Huang, Synthesis, characterization and magnetic properties of β-MnO_2 nanorods, Powder Technol. 154 (2005) 120-124.

[35] J.-J. Feng, P.-P. Zhang, A.-J. Wang, Y. Zhang, W.-J. Dong, J.-R. Chen One-pot hydrothermal synthesis of uniform β–MnO_2 nanorods for nitrite sensing, J. Colloid Interf. Sci. 359 (2011) 1-8.

[36] G. Xi, Y. Peng, Y. Zhu, L. Xu, W. Zhang, W. Yu, Y. Qian, Preparation of β-MnO_2 nanorods through a γ-MnOOH precursor route, Mater. Res. Bull. 39 (2004) 1641-1648.

[37] Y. Wu, L. Guo, Z. Ma, Y. Gao, S. Xing, Structural and morphological evolution of mesoporous α-MnO_2 and β-MnO_2 materials synthesized via different routes through $KMnO_4/H_2C_2O_4$ reaction, Mater. Lett. 125 (2014) 158-161.

[38] M. Sun, B. Lan, L. Yun, F. Ye, W. Song, J. He, G. Diao, Y. Zheng, Manganese oxides with different crystalline structures: Facile hydrothermal synthesis and catalytic activities, Mater. Lett. 86 (2012) 18-20.

[39] F. Li, J. Wua, Q. Qin, Z. Li, X. Huang, Facile synthesis of γ-MnOOH micro/nanorods and their conversion to β-MnO_2, Mn_3O_4, J. Alloy. Compound. 492 (2010) 339-346.

[40] N. Sui, Y. Duan, X. Jiao, and D. Chen, Large-Scale Preparation and Catalytic Properties of One-Dimensional α/β-MnO_2 Nanostructures, J. Phys. Chem. C 2009, 113, 8560-8565.

[41] C. Yu, G. Li, L. Wei, Q. Fan, Q. Shu, J. C. Yu, Fabrication, characterization of β-MnO_2 microrod catalysts and their performance in rapid degradation of dyes of high concentration, Catal. Today 224 (2014) 154-162.

[42] T. Gao, H. Fjellvåg, P. Norby, A comparison study on Raman scattering properties of β- and α-MnO_2, Anal. Chim. Acta 648 (2009) 235-239.

[43] M. Sun, B. Lan, L. Yun, F. Ye, W. Song, J. He, G. Diao, Y. Zheng, Manganese oxides with different crystalline structures: Facile hydrothermal synthesis and catalytic activities, Mater. Lett. 86 (2012) 18-20.

[44] T. Gao, H. Fjellvåg, P. Norby, Structural and morphological evolution of β-MnO_2 nanorods during hydrothermal synthesis, Nanotechnology 20 (2009) 055610.

[45] S. Devaraj and N. Munichandraiah, Effect of Crystallographic Structure of MnO_2 on Its Electrochemical Capacitance Properties, J. Phys. Chem. 112 (2008) 4406-4417.